Automatic three-dimensional features extraction: The case study of L'Aquila for collapse identification after April 06, 2009 earthquake

Valerio Baiocchi[1], Raffaella Brigante[2], Donatella Dominici[3], Maria Vittoria Milone[1]*, Martina Mormile[1] and Fabio Radicioni[2]

[1]'Sapienza' University of Rome, DICEA, Department of Civil and Environmental Engineering, Via Eudossiana 18, Rome, Italy
[2]University of Perugia, DICA, Department of Civil and Environmental Engineering, Via G. Duranti 93,06125, Perugia, Italy;
[3]University of L'Aquila, DICEAA, Via Giovanni Gronchi 18 (Zona industriale di Pile), 67100, L'Aquila, Italy

*Corresponding author, e-mail address: mariavittoria.milone@uniroma1.it

Abstract

This paper illustrates an innovative methodology for post-earthquake collapsed building recognition, based on satellite-image classification methodologies and height variation information. Together, the techniques create a robust classification that seems to yield good results in this application field. In the first part of this study, two different feature extraction methodologies were compared, based respectively on *pixel-based* and *object-oriented* approaches. Then the classification results of the most accurate classification methodology, obtained on an eight band WorldView-2 monoscopic image, were completed with height variation information before and after the event. The height difference is calculated, comparing a photogrammetric DSM, obtained using a photogrammetric rigorous orbital model on some EROS-B 0.7 metre across-track stereopairs with a 'roof model' before the earthquake.
Keywords: image classification, L'Aquila earthquake, collapses, EROS-B, World-View-2.

State of the art

The seismic events that have recently affected many areas of the planet highlight the need to respond to emergencies in a rapid and effective way. To understand and possibly mitigate their impact, particularly on human beings, research is being conducted for each of the characteristic phases of such events, i.e., before the event (early warning systems, risk assessment), during the event (disaster-alerting systems), immediately after the event (emergency response, impact assessment), and during the reconstruction phase (planning of the make safe and restoration). Rapid impact assessment after a catastrophic event is

crucial for initiating effective emergency response actions, and remote sensing data seem to provide important information about the affected areas, since it can quickly map the regions of interest [Brunner et al., 2010]. The use of remote sensing within the domain of natural hazards and disasters has become increasingly common, due in part to the increased awareness of environmental issues such as climate change, but also to the increase in geospatial technologies [Joyce et al., 2009]. For example, information regarding the impact of an earthquake can be derived from satellite imagery by comparing data from a chosen reference before the event (pre-event) to imagery acquired immediately after the event (post-event). Remote sensing has been used in the field of earthquake research since the 1970s, with the first appearance of satellite images [Tronin, 2006], but the methodologies performed in previous decades can now be optimised, thanks to the availability of very high resolution satellite imagery.

For example, the analysis of seismic contest can be performed using SAR (in particular inSAR techniques) imagery to consider and evaluate changes in the backscatter coefficient and intensity [Singhroy, 1995].

According to the literature, an analysis of the consequences of past events can suggest proper strategies to mitigate seismic risk [Terenzio et al., 2013]. In the recent past, specific infrastructures were developed to manage data for early damage assessment in a post-seismic scenario. One such instance was the case of the Bam earthquake, during which the Earthquake Engineering Research Institute (EERI) field team deployed the VIEWS (Visualizing Impacts of Earthquakes With Satellites), a portable reconnaissance system that streamlines and accelerates damage survey activities. VIEWS integrated a base layer of georeferenced satellite or airbourne imagery collected before and after the event with real-time GPS readings; georeferenced digital photographs and/or video; and other geospatial datasets, including damage maps and street networks [Adams et al., 2005]. During a post-seismic period, surveying with classical topographic instruments is often complex because of the possible danger in the area. Although the use of aerial photogrammetry might be less dangerous, it could not, in most cases, produce detailed and accurate information about damaged structures such as facades, even if oblique images may be sued for surveying buildings. Consequently, in recent years, some studies on the use of UAV (Unmanned Aerial Vehicles) for surveying were performed by different research groups. The UAVs do, in fact, detect areas of small extensions; moreover, they do so in short time frames and with reduced costs. As a result, they are more often used for data collection in areas affected by earthquakes, landslides, subsidence, avalanches, or forest fires [Bendeaet al., 2008; Adams et al., 2011; Baiocchi et al., 2013]. In fact, UAVs are valuable sources of data for inspection, surveillance, and 3D modelling issues [Nex et al., 2014].

Change detection on high-resolution satellite images still remains the primary technique used in these situations because it allows a large number of images to be made available in a short amount of time. This essential application of remote sensing technology has been studied and applied since the 1980s; its technique consists of high or very high resolution satellite image processing for the detection and/or discrimination of changes in both environmental and anthropic context over time [Singh, 1989; Lu et al., 2014]. Many types of change detection methods are included in multi-spectral image data, but the most utilised ones are based on image classification, whereby it is possible to individuate collapsed buildings affected by earthquakes by considering the difference between their

spectral signature and those of undamaged ones. The classification could be performed with pixel-based traditional algorithms or object-oriented techniques. However, several previous studies have revealed that pixel-based algorithms sometimes fail to recognise collapses. For this reason, after the Kobe earthquake of 1995, Yamazaki [2001] tested a context-based approach, which simulates the human perception for damage detection. Although literature abounds with various speculation about the problems affecting the pixel-based approach [Cracknell, 1998; Blaschke, 2010], the authors all agree that, in many applications, the approach based on comparing single pixels could be ineffective.

Other authors have already explained the disadvantage of traditional methods that provide only a two-dimensional (2D) damage change of the collapsed buildings, and have underlined the importance of detecting collapsed buildings in an earthquake with a 3D-based approach. In other words, it would be more effective to consider the height change of the buildings by using pre- and post-seismic stereo image pairs. Tong et al. [2012] used this approach on the case study of the May 2008 Wenchuan earthquake, using Ikonos stereopairs. The accuracy of better than 1.1 m in planimetry and 1.5 m in height that can be achieved, as the authors stated, from the pre- and post-seismic Ikonos stereo image pairs guarantees the feasibility of detecting 3D geometric changes in the earthquake-induced building collapses from pre- and post-seismic HRSI stereo images [Tong et al., 2012]. Also, DSMs from aerial imagery were tested [Turker et al., 2005] for the detection of the collapsed buildings by using digital elevation models (DEMs) before and after the earthquake. In this study, the two digital models were compared once they were extracted, and the obtained height difference was analysed building by building to detect where it exceeded a specified threshold level between pre- and post-earthquake measurements.

Baiocchi et al. [2010] developed research on the Umbria-Marche (Italy) earthquake (09/26/1997) by using both techniques. In particular, they compared DSM extracted from aerial (before) stereopairs and Ikonos (after) stereopairs, evidencing that some false detections were due to errors in correlation and interpolation of both DEMs.

The present paper will illustrate the advantages of combining several satellite image classification methodologies with height variation information to better identify collapsed buildings after an earthquake. There are several benefits to the combined use of these two techniques. Using only the change detection is not always effective for these applications because a collapsed building may have the same radiometry as an undamaged one, while the height differences should optimise the recognition of collapses. To reduce false height-difference effects, the height of the pre-event situation was acquired from vectorial information. This information was restricted to the areas where building presence was reported, and was obtained using a digital elevation model of the roofs only.

As previously stated, in recent years, growing attention has been paid to remote sensing and GIS when used for disaster management applications [Zlatanova, 2008; Boccardo, 2013]. For this reason, the test area has been designated as L'Aquila city, in the Abruzzo region of Italy. This city was struck by a series of earthquakes in April 2009, devastating its historic centre and the surrounding area. This event destroyed or seriously compromised a significant cultural and historic heritage, the protection of which will factor heavily in the reconstruction planning. In addition to the 300 victims and 1,500 wounded, the earthquake damaged about 15,000 buildings, including landmarks in the city such as the

Palace of the Prefecture, the dome of the church of Anime Sante, the Student House, and the churches of Santa Maria Paganica and the Santa Maria di Collemaggio (the last is protected by UNESCO). The city centre was secured, but its restoration has only begun (May 2014).

Data and methods

For the test area, a very high resolution WorldView-2 satellite monoscopic image was acquired. The new generation of VHR optical images (≤ 1 m), such as WorldView-2, enable the detection of minute changes on the surface; they also introduce some new problems related to the large amount of information being gathered, which were not encountered with the previous sensors [Dell'Acqua et al., 2011]. The image displayed in Figure 1 was acquired on August 9, 2010, a few months after the main seismic event took place. It covers about 50 km^2 of the historical centre of the city, extending also to rural and peripheral areas.

Figure 1 - WorldView-2 image of L'Aquila (figure is approximately 50 Km^2).

To complete the classification, height information was extracted from DSM obtained from an across-track stereopair of L'Aquila acquired by the EROS-B satellite on April 17, 2009 and April 24, 2009, just a few days after the main seismic event (Fig. 2). Actually, the images utilised cannot be properly defined as stereopairs because they are, in effect, two single monoscopic acquisitions taken on two consecutive days; but because of its relative geometric similarity to a stereoscopic acquisition, it can be considered similar to an actual across-track stereopair; in previous papers, authors [Baiocchi et al., 2013] described the acquisitions as *pseudostereopairs*, but to avoid possible confusion, they will be referenced in this paper as *across-track stereopairs*.
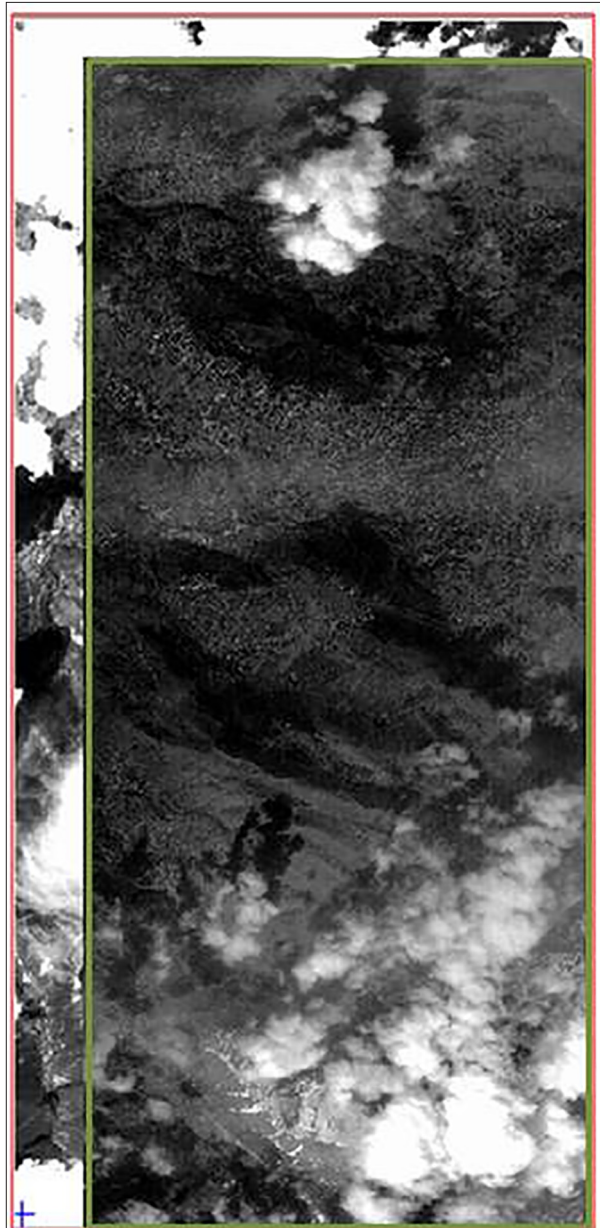
Figure 2 - Eros-B across-track stereopair of L'Aquila.

To perform a classification on a monoscopic satellite image, it is mandatory to use a pansharp image [Parente and Santamaria, 2013], an image that has the geometric resolution of pancromatic band and the color of multispectral ones. Thus, once obtained, we orthorectified the pansharpened image using 22 GPS/GNSS RTK control points equally distributed on the frame and a digital elevation model obtained from 1:5000 scale regional technical cartography. The expected planimetric and altimetric accuracies

were, respectively, 0.05 m and 0.10 m for GCPs (Ground Control Points) and 1.0 m and 3.5 m for cartography. Considering the extension and the heterogeneity of the study area, we divided the image into 9 subsets, approximately 2.3 x 2.3 km each, as shown in Figure 3.This step is often recommended in order to reduce the processing time required by high-dimension images, but also to optimise the classification according to different characteristics of each subset.
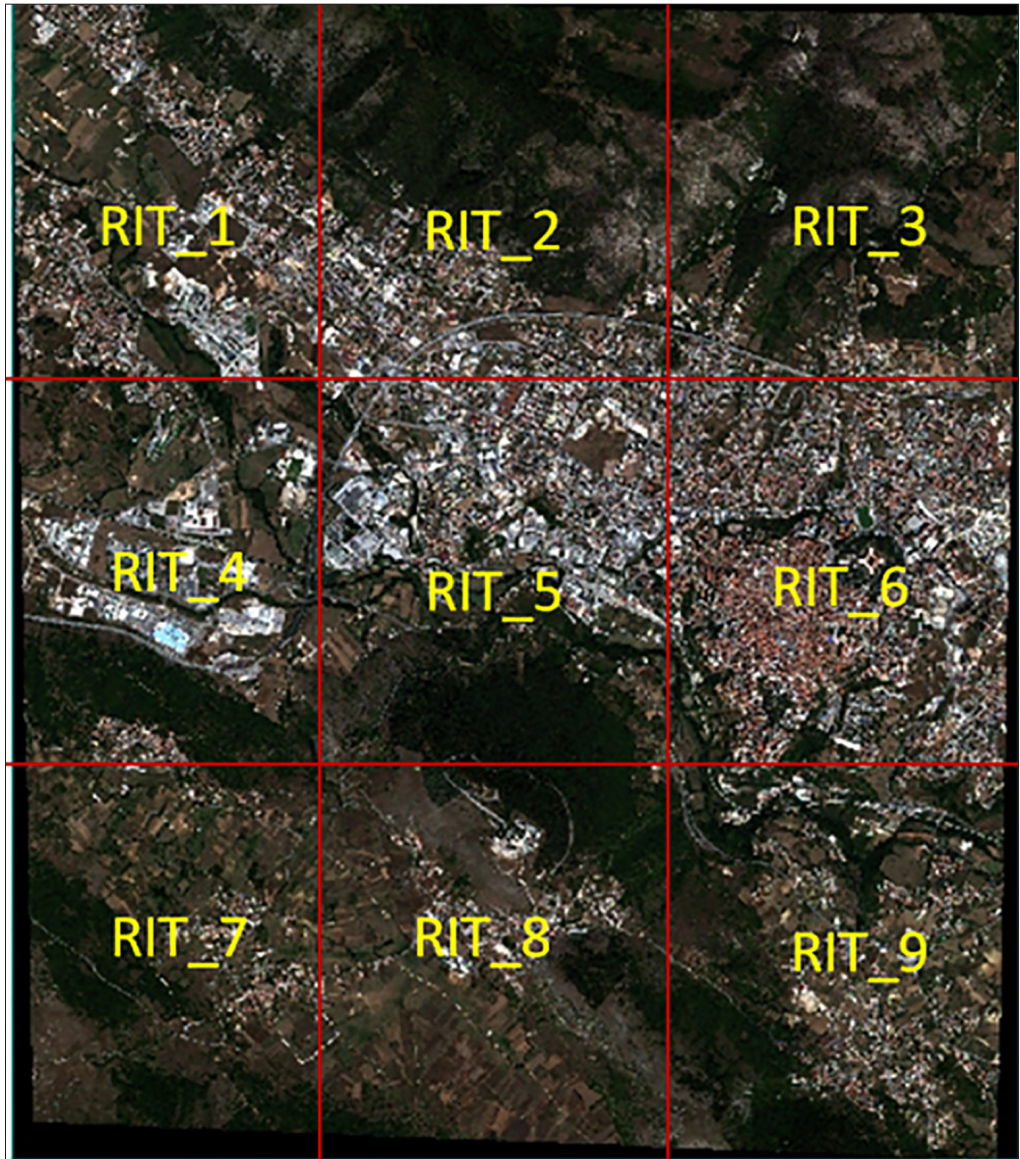

Figure 3 - The 9 subsets of WorldView-2 image.

We then performed the classification with two algorithms: the *object-oriented* approach as implemented in eCognition Developer 8.0 and the *pixel-based* approach, implemented in the software Envi Ex. The adopted class hierarchy was the same for both cases and for each subset of images, to allow for a reliable comparison of the final results. A list of the classes and relative subclasses is provided in Figure 4.
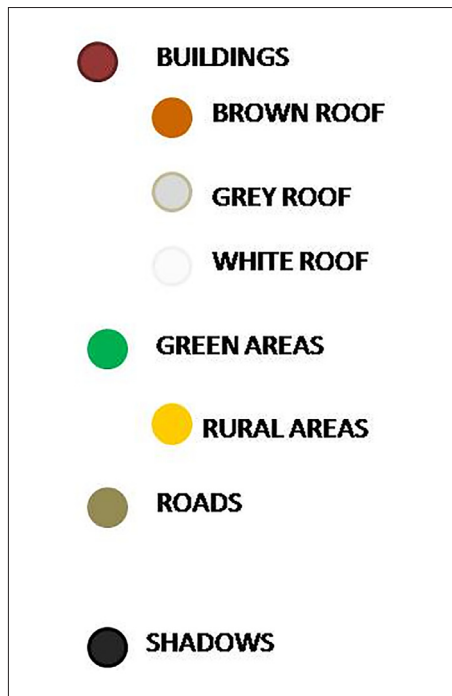

Figure 4 - The classes and subclasses identified in the image (class hierarchy).

The object-oriented approach toward image analysis is based on the idea that the important information necessary to interpret an image is not represented only in a single pixel, but in meaningful image objects and their mutual relationships. The basic difference, especially with regard to pixel-based procedures, is that this technique doesn't classify single pixels, but rather image objects that are extracted in a previous image segmentation step; that is, it uses a bottom-up, region-growing technique, starting with one-pixel objects. Starting at an arbitrary point in the image with one-pixel objects, and in a number of consecutive steps, the pixel objects are enlarged to bigger pixel groups (segments) until certain heterogeneity is reached. The obtained segments are optimised using three homogeneity criteria: scale, shape, and color. Obviously, the scale parameter, which defines the mean dimension of the image object identified, plays a fundamental role in the robustness of the classification [Al-Khudhairy et al., 2005]. Indeed, the scale parameter must be chosen according to different situations and goals. For this reason, in this experiment, we tested the segmentation results

obtained using different scale parameters (Fig. 5), and approximately considered the target object dimension that corresponds with the dimensions of the roof of a building.
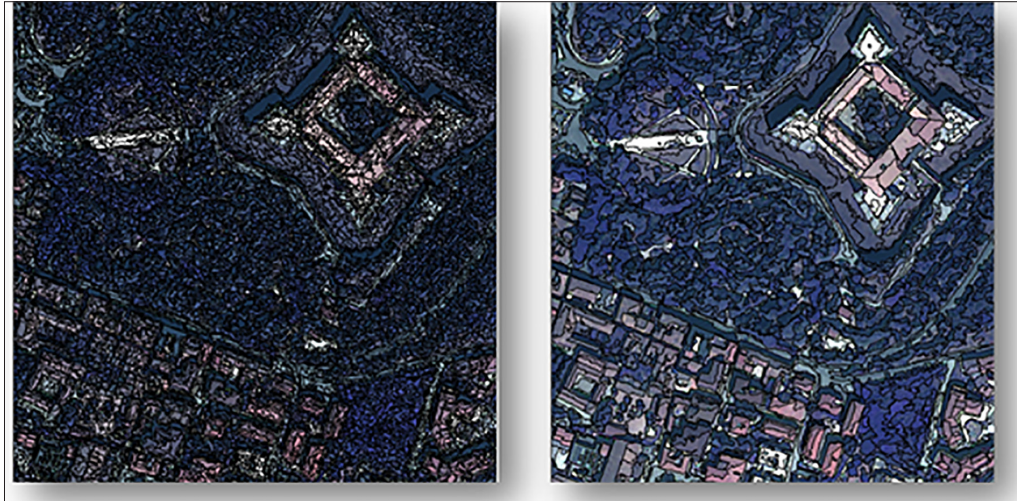

Figure 5 - Results of segmentation with different scale parameters (20 and 60) performed on a subset of image.

For the present study and imagery used, a scale parameter of 60 seemed to result in the best performance, but this can only be considered as a tentative guideline for future experimentations because several tests should be performed to find, case by case, the scale that best fits the specific application for the image.

The processing time of the segmentation obviously depends on the number of image objects that have to be created during the segmentation; again, it depends mainly on the scale parameter. In the example reported in this paper, with a scale parameter of 60, the processing time for each 2.3 x 2.3 km subset was about two minutes.

After the segmentation, the classification could be performed in different ways and through different steps. In this case, because attention had to be focused on the buildings class, we decided to begin by classifying all of the vegetation using classical NDVI criteria. The NDVI (*Normalised Difference Vegetation Index*), as it is well known, is calculated from the visible and near-infrared light reflected by vegetation [1].

$$NDVI = \frac{(NIR - VIS)}{(NIR + VIS)} \quad [1]$$

Calculations of NDVI always result in a number that ranges from minus one (-1) to plus one (+1); however, the absence of green leaves gives a value close to zero. A value of zero implies an absence of vegetation, and a value close to +1 (0.8 – 0.9) indicates the highest possible density of green leaves. In this case, the NDVI feature was created by combining

channels 5 (red channel) and 7 (near infrared channel) of the WorldView-2 image. Then a threshold was chosen to accurately assign the objects to the vegetation class for the specific characteristics of the images; one must remember that, due to the elevated number of bands (8) in this satellite, the interval in each single band is different from that of the most diffused, four-band satellites [Padwick et al., 2013].The result obtained from the NDVI classification is displayed in Figure 6.

Figure 6 - Classification of vegetated areas through NDVI.

A detailed explanation of this phase is omitted from this article for issues of length, but a complete description can be found in a previous paper [Baiocchi et al., 2013]. A literature review revealed the concern that use of the NDVI for the elimination of vegetation from further data processing steps carries the risk that the shadowed parts of the buildings will also be eliminated from the processing [Grigillo et al., 2011]. For this reason, the same procedure was used to classify the shadows in the image. In this case, a predefined feature of brightness was used, so after the most appropriate threshold of brightness was chosen, the unclassified objects from previous classifications were assigned to the shadows class (Fig. 7).

For all other classes in our hierarchy, we adopted a nearest-neighbour classification because this has been deemed a proven and robust classifier. In fact, by considering identified samples as representatives for each class, the algorithm searches for the closest sample object in the feature space for each image object. In some cases, we completed the class description by designating specific parameters. For example, for the buildings class, we added a threshold regarding the extent (area > 80 m²), while for the shadows, we inserted a condition about the proximity to other classes such as vegetation or buildings (distance to buildings < 2 m). The selected samples are shown in Figure 8; it is imperative that this

operation be performed manually by selecting the appropriate number of samples, which usually seems to be correlated to the total number of image objects created during the segmentation; furthermore, the samples must be equally distributed over the entire image. In Figure 9, the results of the classification for two subsets of our image are shown.

During the present experimentation, the nearest-neighbour classification phase varied with regard to the processing time, depending on the category being classified, the features selected, and so on; as the rule sets increased in complexity, so did the time needed to complete the classification.

Figure 7 - Classification of shadows through brightness features.

Usually, this process took between 30 min and 60 min for each subset of the image. Following the classification, the rule-set was applied, with small changes made to all subsets of the image; Figure 10 shows the vector file of polygon buildings, with the same file overlaid with the satellite image.

The same class hierarchy was adopted for the second algorithm (pixel-based approach). For each class, we selected representative pixels; thus, this procedure is called the supervised pixel-based classification. The classification algorithm identified the pixels belonging to the various classes, according to the maximum probability of belonging to the class. As in the previous case, the vegetation was identified automatically by exploiting the spectral response in the different bands, especially through the vegetation index NDVI, combining bands of red and near infrared. The results obtained are shown in Figure 11.
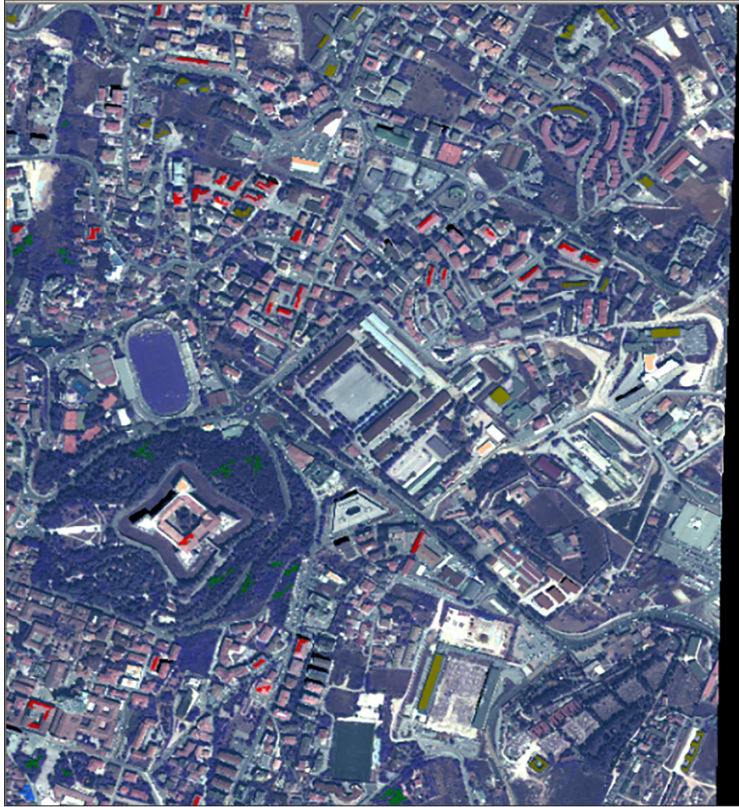
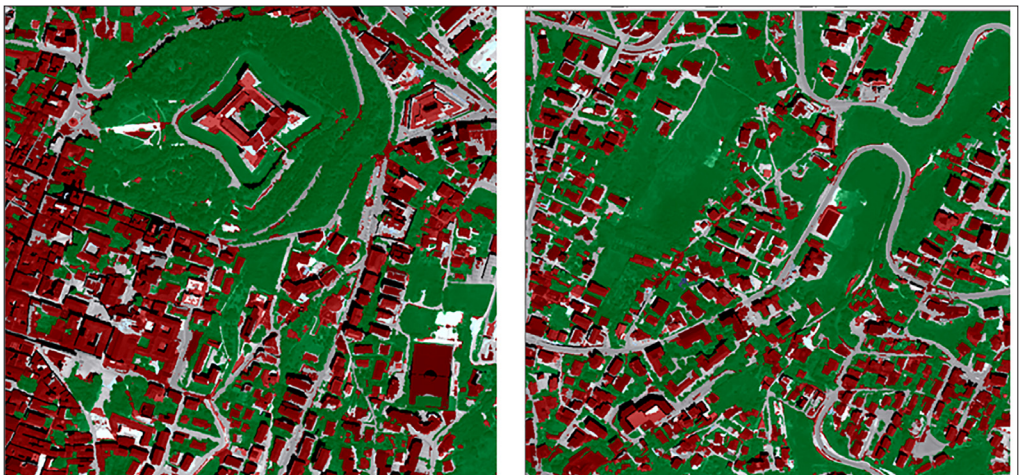**Figure 8 - Samples selected for each class of class hierarchy.**

Figure 9 - Classification results (object-oriented approach) on some subsets (red for buildings, gray for streets, green for vegetated areas, and black for shadows).
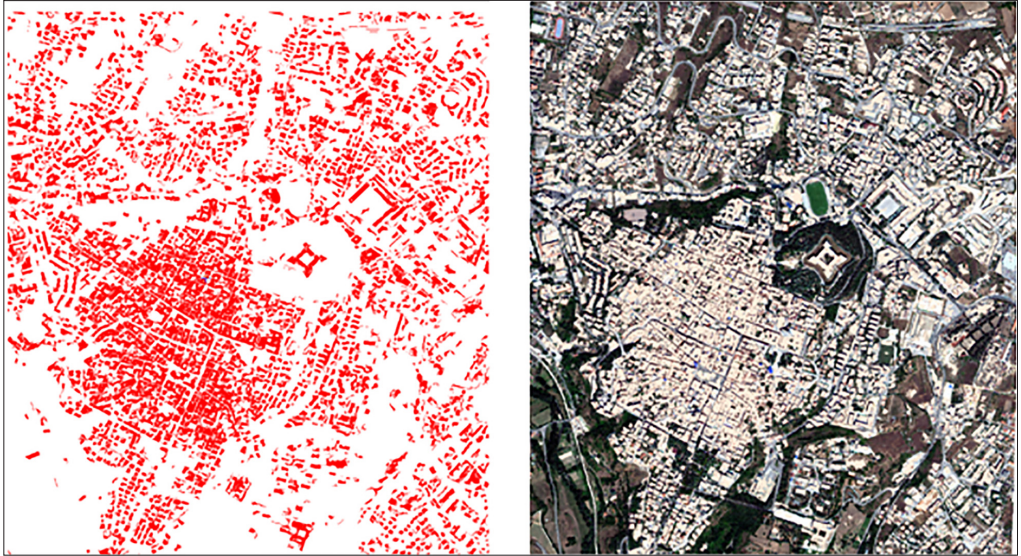
Figure 10 - The vector file of buildings obtained after the image classification (left) and the same file overlapped to a satellite image (right).
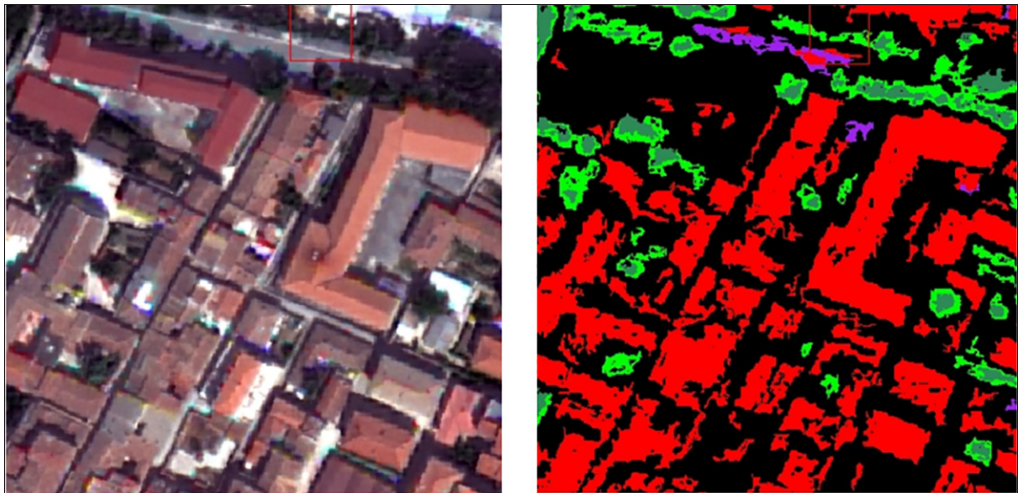

Figure 11 - Pixel-based classification results of some subsets (historic centre of L'Aquila).

Our purpose was to complete the classification results for height information, so we tried to identify collapsed buildings by considering their height differences from before and after the earthquake. For this reason, we decided to compare the pre- and post-seismic events model. The DSM before the main seismic event was extracted by 1:5000 vectorial cartography, considering only the polygons of the buildings through a rasterisation process in the GIS environment (referred to as *roof model*), as shown in Figure 12.
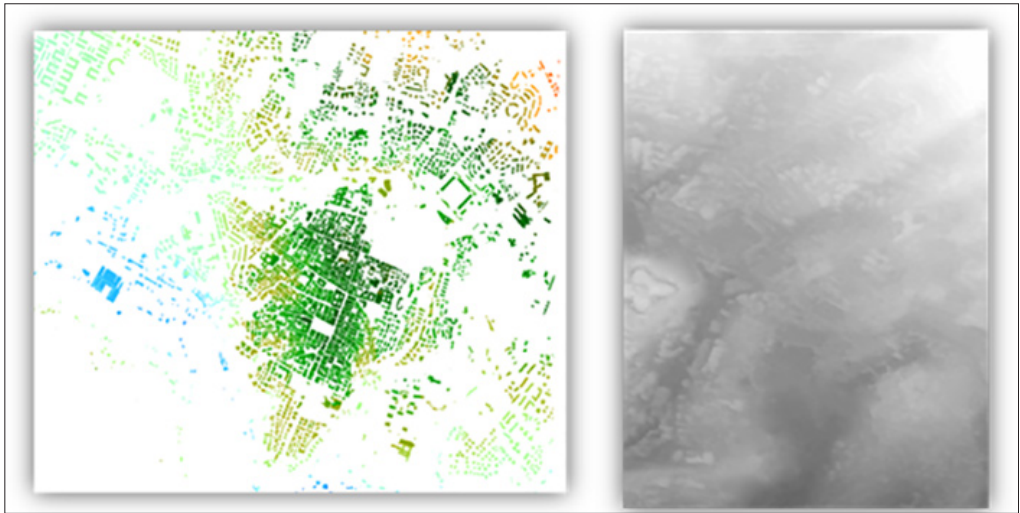
Figure 12 - Digital Surface Model before (left) and after (right) the earthquake.

The model of the post-seismic period was obtained from the EROS-B across-track stereopair of L'Aquila city .The differences of both models in Figure 12 are obviously due to the different methods used to obtain them. For more detail on the DSM extraction, see Baiocchi et al., 2013. In short, we performed the DSM extraction with PCI software and implemented Toutin's rigorous model [Poli and Toutin, 2012]. We oriented the two across-track stereopair images using a set of GCPs and CPs (Check Points). After that, observing the RMSE of GCPs and CPs while increasing the number of GCPs, we estimated both the precision and accuracy, which seemed to stabilise around 0.5 m – 1.0m of RMSE in the first case and 3.0 m –3.5 m of RMSE in the second. Following the DSM extraction, to validate the model, we compared the height of the spot points in the 1:5000 vectorial cartography of L' Aquila with those in the obtained DSM.

Classification results and collapses recognition

To evaluate the classification results obtained with both algorithms and assess their accuracy, we decided to reference the existing buildings by using the 1:5000 scale cartography ("CartaTecnicaRegionale", CTR), realised by the Abruzzo regional administration. The objects on the polygonal vectorial file of this cartography, identified in the associated database as buildings (e.g., "Religious buildings" and "Civil buildings"), were considered to be the only buildings existing in L'Aquila city before the main seismic event. Even if the cartography wasn't updated after 2004, the urban changes occurring between the last update of the CTR and the acquisition of WorldView-2 image would be minor because L'Aquila is a historic city centre; thus, the construction of new buildings is forbidden. Moreover, the first phases of early damage assessment are usually conducted by Civil Protection, using the available cartography; in fact, these exact maps were used during the L'Aquila earthquake.

First of all, we compared the effectiveness of both classification algorithms and evaluated their respective results by comparing them to the buildings on the cartography. Collapsed

buildings were ignored because they are a very small portion of all the buildings in the historic centre. We also conducted other evaluations in the GIS (Q-GIS) environment. For example, we compared the areas of the buildings both on the CTR and from classifications algorithms (object-oriented and pixel-based) in order to evaluate the recognition percentage of the approaches used and their validity. The obtained results are reported in Tables 1 and 2.

Table 1 - Comparison to official cartography (Object-oriented).

	Buildings of cartography detected by classification	Buildings of cartography	Recognition percentage
	(m²)	(m²)	%
SUB_1	304648.2	328212.8	92.8
SUB_2	180655.6	198266.8	91.1
SUB_3	60202.1	72486.2	83.1
SUB_4	66550.6	77133.4	86.3
SUB_5	305229.8	324835.0	94.0
SUB_6	973265.6	1031172.2	94.4
SUB_7	56030.1	62386.9	89.8
SUB_8	80642.0	86255.0	93.5
SUB_9	157253.5	168111.4	93.5
Total	2184477.4	2348859.6	93.0

Table 2- Comparison to official cartography (Pixel-based).

	Buildings of cartography detected by classification	Buildings of cartography	Recognition percentage
	(m²)	(m²)	%
SUB_1	179251.3	328212.8	54.6
SUB_2	58029.9	198266.8	29.3
SUB_3	32454.9	72486.2	44.8
SUB_4	115946.5	77133.4	60.3
SUB_5	247367.3	324835.0	76.2
SUB_6	692349.9	1031172.2	67.1
SUB_7	23907.2	62386.9	38.3
SUB_8	46206.7	862545.0	53.6
SUB_9	101974.5	168111.4	60.7
Total	1497488.4	2348859.6	63.8

Clearly, the object-oriented classification is more accurate and robust; it achieved a substantial recognition percentage (over 93%), whereas the pixel-based approach reached a percentage of 63%. The recognition percentage of the pixel-based approach for some

subsets seems to be exceedingly low, in fact, marking this approach as an ineffective means for buildings identification. For this reason, we decided to use only the results obtained with the object-oriented classification for the following analysis.

By overlapping the vectorial file of the buildings identified by the classification on the buildings of the CTR with those on the satellite image, we could immediately identify some collapses, such as that of Santa Maria Paganica Church (Fig. 13).
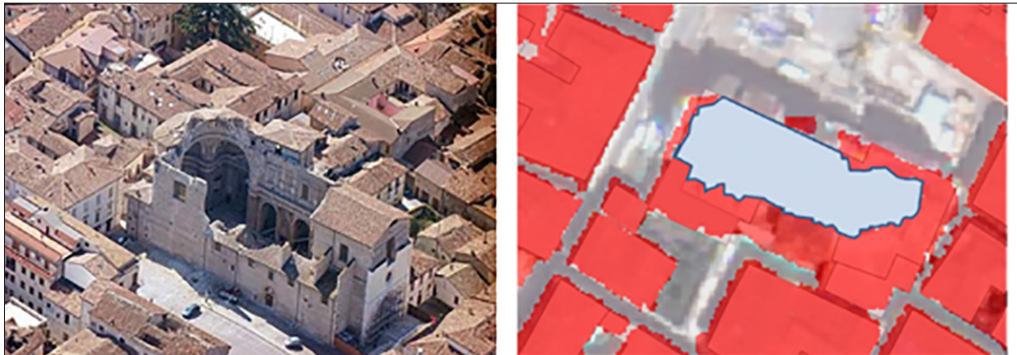

Figure 13 - The identified collapse of Santa Maria Paganica Church with classification.

A significant subset of the images was selected for subsequent experimentations, and based on this area, we made several calculations (Tab. 3):

1) The total number of buildings on the official cartography;
2) The number of buildings reported on CTR but not identified by the classification algorithms (these could be collapsed buildings after the earthquake);
3) The number of buildings identified by our classification algorithms but not present on CTR (If such buildings exist, they might be "new buildings," erected after the cartography's last update).

Table 3 - Results of collapses recognition: comparison between classification and cartography buildings.

Total number of buildings (classification and cartography)		756		100%
Buildings on cartography		751		99.3%
Buildings present on cartography but not identified by classification algorithms	9	Classification mistakes	6	1.2%
		Collapsed buildings	3	
Buildings identified by classification algorithms but not present on cartography	14	Classification mistakes	9	1.85%
		Cartography limits	5	

With regard to the third calculation, 9 probable "new buildings" were actually classification mistakes (the classification algorithms seem to incorrectly classify shadows or paved areas

as buildings because they share a similar radiometry to the roofs; Fig. 14) while 5 buildings were not present on the CTR. The latter buildings weren't new because the area is a historic centre; most likely, they were not classified as 'Buildings' in the database linked to the official cartography.

Figure 14 - Classification mistakes; the algorithms (red color) classify some paved areas as buildings not present in CTR buildings (yellow color).

Regarding the 9 probable collapsed buildings identified by the classification, 3 were actually collapsed buildings (for example, Fig. 15) while the other 6 were classification mistakes; in this case, the algorithms may have assigned some buildings' image objects to another category.

Figure 15 - Buildings collapsed and not identified by classification algorithms (red color)but reported on cartography (yellow color).

One should note, however, that the identified collapsed buildings are the only buildings that really collapsed in the area.

The aim of this study was to complete the classification results with DSM information in order to achieve a more robust identification of collapsed buildings and to consider height differences of buildings before and after the earthquake. Thus, we calculated the difference between these two models and focused on the greatest differences (red color in Fig. 16) between the DSM height and that extracted from the cartography in polygon buildings, obtaining a model that provides information about the elevation where an edifice is present, but does not provide data about the elevation where no construction is present; in a certain way, this model can be considered as a "roof model." This approach can be an improvement of the use of "normalised DSM" (nDSM) proposed by some authors [Weidner, 1997] and give more accurate results, but the weak point is that it can be used only when a large scale (1:10000 or better) vectorial cartography is available.
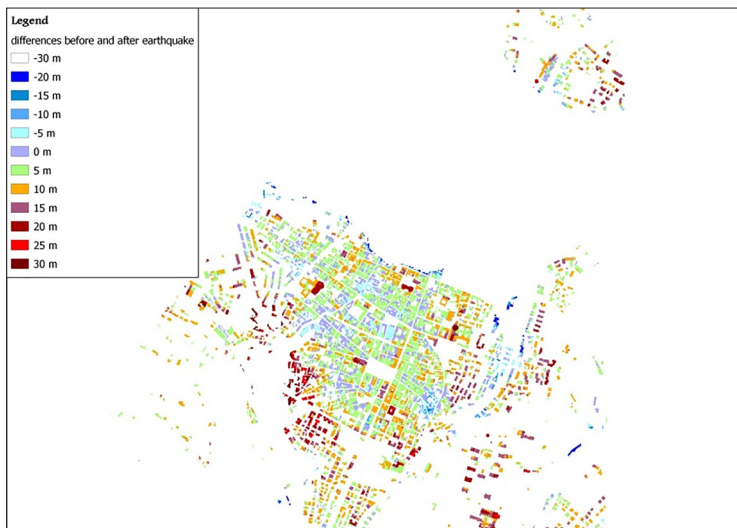

Figure 16 - Differences obtained between DSM from across track stereopair and roof model.

In the same subset of previous tests, the methodology reveals 6 possible collapses: 3 are actual collapses (for example, Fig. 17), whereas the remaining differences between pre- and post-earthquake models are due to some misclassification.

This methodology did report false detections of collapsed buildings, mainly because the particular shape and structure of some buildings were not properly depicted (Tab. 4) by the vectorial cartography used to obtain the model before the earthquake. The details in Figure 18 show the false detection of buildings with high height differences that are not collapsed. This is due to the fact that in Italy, 1:5000 scale maps represent the roofs as polygons with unique heights and flat surfaces; higher scale maps (e.g., 1:2000) are expected to include more complex roof shapes but, unfortunately, the 1:5000 scale maps offer the only altimetric documentation of the entire city centre of Italy; thus, they are the only sure source of altimetric information available for civil protection purposes.

Figure 17 - The identified collapse of Santa Maria Paganica Church with height differences.
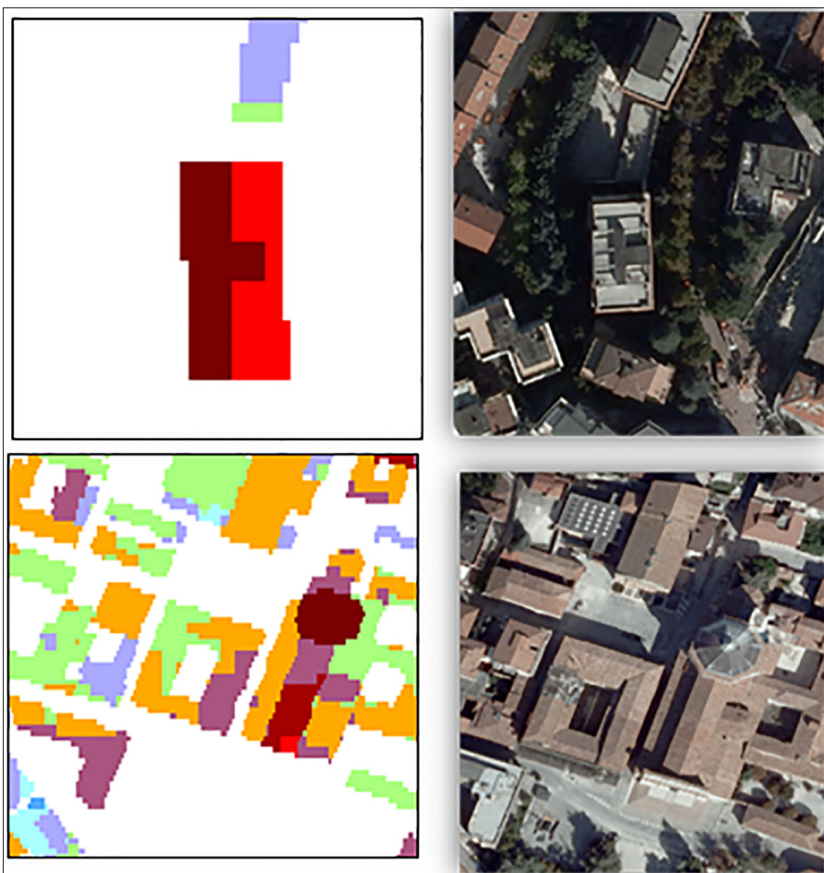

Figure 18 - Examples of false detection with the technique of height differences.

Significantly, the 3 collapsed buildings that were detected with both methodologies, due to the radiometry and altimetry, are the only ones that could be visually detected. This consideration confirms the speculation that the proposed procedure is able to automatically detect, with considerable time saved, all collapsed buildings that could be optically identified. For this reason, it could be compared to the most diffused "early damage assessment" methodologies presently in use.

Table 4 - Results of collapses recognition: comparison between height information and cartography buildings.

Buildings with high differences of height between pre-and post-earthquake DSM	6
Building collapses	3
Methodology mistakes	3

We tried to better evaluate the accuracy of our methodologies by comparing their results to the actual verified damages detected by the Civil Protection and Fire Department operators after the event; In Italian, these inspections are called "Agibilità," and the authors think a translation of this word can be "Fitness for human habitation," because the result of every building inspection determines if the building is still usable for habitation or not. The results of this verification are available for free on the "Fitness for human habitation" map [Comune L'Aquila, 2013] (Fig. 19), which displays a representative subset of the image.
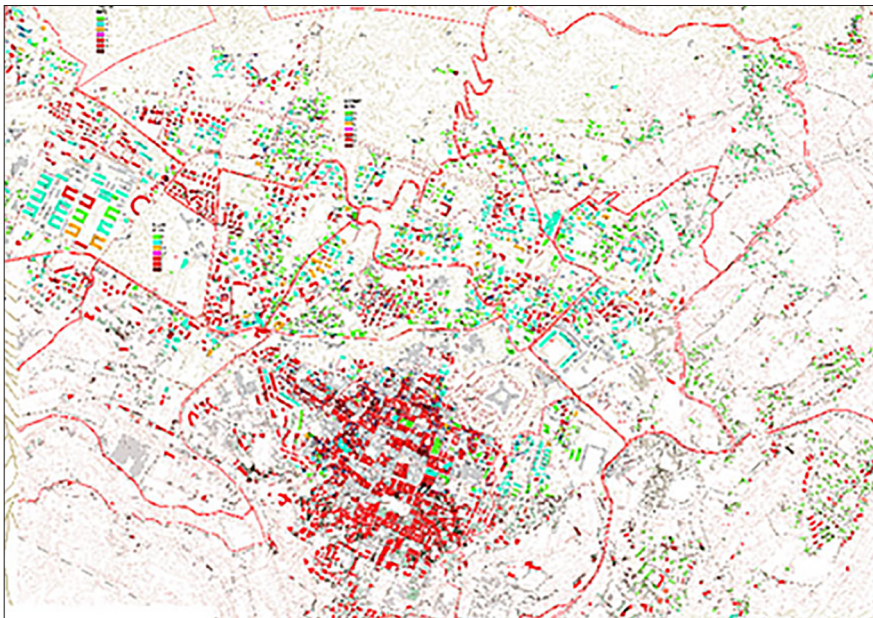

Figure 19 - The map of fitness for human habitation made by Civil Protection after the main seismic event.

The results of these tests, performed in an open-source, GIS environment, and using "map algebra" algorithms, are shown in Table 5.

Table 5 - Results of collapses recognition: comparison with fitness for human habitation map.

Buildings classified as collapsed or seriously damaged in fitness for human habitation map	6
Building collapses	3
Buildings not totally collapsed but seriously damaged	3

Fitness for human habitation does not directly connect to the collapse of buildings; in fact, an edifice that has not collapsed can be useless for human habitation due to structural damages that can potentially lead to a collapse. We compared these two classifications because of the obvious correlation between them, although these are two conceptually different assessments. Also, this map offers the only available information on the field validation of the damage because admittance to the so called "Red zone," the Zone of the historic centre most damaged by the event and for this reason inaccessible, is still logistically difficult.

Our methodology identifies only 3 collapsed buildings of the 6 classified as "very seriously damaged or collapsed" in the fitness for human habitation map of the same subset; most likely, the remaining 3 buildings are not totally collapsed, and for this reason, not visible on the WorldView-2 image. Indeed, a visual check of these buildings on the WorldView image confirmed that, on the image itself, there is no visual evidence of the collapse.

Conclusions and further development

This research showed that the use of a high-resolution, object-oriented classification image combined with difference-of-height data can accurately, quickly, and robustly detect changes in post-seismic scenarios. The object-oriented approach, in particular, seems much more accurate with 93% recognition, compared to the 64% recognition reported by the pixel-based classification. In this experimentation, in fact, all of the totally collapsed buildings were identified by the object-oriented approach. Some mistakes during the classification process could be avoided through an optimisation of the process and improved specialisation of the implemented rule-set. Since optimizing the DSM extraction from satellite stereopairs and obtaining even more accurate height information will improve the classification, deeper investigations must be conducted. Clearly, the proposed methodology must be tested more widely on this and other post seismic scenarios; nonetheless, this study determined that the detection of post-earthquake collapsed buildings can be substantially enhanced by combining these two techniques, resulting in a complete detection of observable collapsed buildings with no errors (from the studied subset). This methodology, therefore, could allow a first damage assessment to be performed quickly in a completely automated way through the use of remotely sensed data, thereby offering ready support for the emergency response activities carried out by humanitarian agencies (Boccardo et al., 2011).To achieve an effective application of such methodologies, a prearranged preparation of the necessary pre-event data is of strategic importance, as is the availability of high-performance hardware to quickly execute classification and DSM extraction in immediate post events.

References

Adams B.J., Mansouri B., Huyck C.K., (2005) - *Streamlining post-earthquake data collection and damage assessment for the 2003 Bam, Iran earthquake using visualizing impacts of earthquakes with satellites (VIEWS).* Earthquake Spectra, 21 (S1): 213-218. doi: http://dx.doi.org/10.1193/1.2098588.

Adams S.M., Friedland C.J. (2011) - *A survey of unmanned aerial vehicle (UAV) usage for imagery collection in disaster research and management.* In "The 9th International Workshop on Remote Sensing for Disaster Response", Stanford University on 15-16 September 2011.

Ajmar A., Boccardo P., Tonolo F.G. (2011) - *Earthquake damage assessment based on remote sensing data. The Haiti case study.* Italian Journal of Remote Sensing , 43 (2): 123-128. doi: http://dx.doi.org/10.5721/ItJRS20114329.

Al-Khudhairy D.H.A., Caravaggi I., Giada S. (2005) - *Structural Damage Assessments from Ikonos Data Using Change Detection, Object-Oriented Segmentation, and Classification Techniques.* Photogrammetric Engineering & Remote Sensing, 71, (7): 825-837. doi: http://dx.doi.org/10.14358/PERS.71.7.825.

Baiocchi V., Brigante R., Radicioni F. (2010) - *Three-dimensional multispectral classification and its application to early seismic damage assessment.*Italian Journal of Remote Sensing, 42 (3): 49-65. doi: http://dx.doi.org/10.5721/ItJRS20104234.

Baiocchi V., Dominici D., Ferlito R. , Giannone F., Guarascio M.,Zucconi M. (2012) - *Test of a building vulnerability model for L'Aquila earthquake.* Applied Geomatics, 4 (2): 95-103. doi: http://dx.doi.org/10.1007/s12518-011-0065-x.

Baiocchi V., Brigante R., Dominici D., Milone M.V. (2013) - *Multispectral automatic feature extraction methodologies comparison.* In Proceedings of '33rd EARSeL Symposium 2013.

Baiocchi V., Dominici D., Milone M.V., Mormile M. (2013) - *Development of a software to plan UAVs stereoscopic flight: An application on post earthquake scenario in L'Aquila city.* Lecture Notes in Computer Science (including subseries Lecture Notes in Artificial Intelligence and Lecture Notes in Bioinformatics), 7974 LNCS (Part 4) :150-165.

Baiocchi V., Dominici D., Milone M.V., Mormile M. (2013) - *DSMs extraction methodologies from EROS-B "pseudo-stereopairs", PRISM stereopairs in coastal and post-seismic areas.* Lecture Notes in Computer Science (including subseries Lecture Notes in Artificial Intelligence and Lecture Notes in Bioinformatics), 7974 LNCS (Part 4):136-149.

Baiocchi V., Dominici D., Giannone F., Zucconi M. (2012) - *Rapid building damage assessment using EROS B data: The case study of L'Aquila earthquake.* Italian Journal of Remote Sensing, 44 (1): 153-165. doi: http://dx.doi.org/10.5721/ItJRS201244112.

Bendea H., Boccardo P., Dequal S., Giulio Tonolo F., Marenchino D., Piras M. (2008) - *Low cost UAV for post-disaster assessment.* In Proceedings of The XXI Congress of the International Society for Photogrammetry and Remote Sensing, Beijing (China) July 2008, pp. 3-11.

Blaschke T., (2010) - *Object based image analysis for remote sensing.* ISPRS Journal of Photogrammetry and Remote Sensing, 65 (1): 2-16. ISSN 0924-2716.

Boccardo P. (2013) - *New perspectives in emergency mapping.* European Journal of Remote

Sensing, 46 (1): 571-582. doi: http://dx.doi.org/10.5721/EuJRS20134633.

Brunner D., Lemoine, G., Bruzzone, L., (2010) - *Earthquake damage assessment of buildings using VHR optical and SAR imagery*. IEEE Transactions on Geoscience and Remote Sensing, 48 (5): 2403-2420. doi: http://dx.doi.org/10.1109/TGRS.2009.2038274.

Comune L'Aquila (2013) - Carta "esiti agibilità" (http://www.comune.laquila.it/pagina79_esiti-delle-verifiche-di-agibilita.html).

Cracknell A.P. (1998) - *Review article Synergy in remote sensing-what's in a pixel?* International Journal of Remote Sensing, 19 (11): 2025-204,. doi: http://dx.doi.org/10.1080/014311698214848.

Dell'Acqua F., Bignami C., Chini M., Lisini G., Polli D., Stramondo S. (2011) - *Earthquake damages rapid mapping by satellite remote sensing data: L'Aquila April 6th, 2009 event*. IEEE Journal of Selected Topics in Applied Earth Observations and Remote Sensing, 4 (4): 935-943. doi: http://dx.doi.org/10.1109/JSTARS.2011.2162721.

Eisenbeiss H., Sauerbier M. (2011) - *Investigation of UAV systems and flight modes for photogrammetric Applications*. The Photogrammetric Record 26 (136): 400-421. doi: 10.1111/j.1477- 9730.2011.00657x.

Grigillo D., Kosmatin M., Petrovič D. (2011) - *Automatic extraction and building change detection from digital surface model and multispectral orthophoto*. Geodetskivestnik, 55:1.

Joyce K.E., Belliss S.E., Samsonov S.V., McNeill S.J., Glassey P. J., (2009) - *A review of the status of satellite remote sensing and image processing techniques for mapping natural hazards and disasters*. Progress in Physical Geography, 33 (2): 183-207. doi: http://dx.doi.org/10.1177/0309133309339563.

Lu D., Mausel P., Brondízio E., Moran E. (2004) - *Change detection techniques*. International Journal of Remote Sensing, 25 (12): 236-2401. doi: http://dx.doi.org/10.1080/0143116031000139863.

Nex F., Remondino F. (2013) - *UAV for 3D mapping applications: a review*. Applied Geomatics, 6 (1): 1-15. doi http://dx.doi.org/10.1007/s12518-013-0120-x.

Padwick C., Deskevich M., Pacifici, F., Smallwood S. (2010) - *WorldView-2 pan-sharpening*. Proceedings American Society for Photogrammetry and Remote Sensing.

Parente C., Santamaria R. (2013) - *Increasing Geometric Resolution of Data Supplied by Quickbird Multispectral Sensors*. Sensors & Transducers, 156, (9): 111-115.

Poli D., Toutin T. (2012) - *Review of developments in geometric modelling for high resolution satellite pushbroom sensors*. The Photogrammetric Record, 27 (137): 58-73. doi: http://dx.doi.org/10.1111/j.1477-9730.2011.00665.x.

Singh A. (1989) - *Review Article Digital change detection techniques using remotely-sensed data*. International Journal of Remote Sensing, 10 (6): 989-1003. doi: http://dx.doi.org/10.1080/01431168908903939.

Singhroy V. (1995) - *SAR integrated techniques for geohazard assessment*. Advances Space Rerearch., 15 : 67-78. doi: http://dx.doi.org/10.1016/0273-1177(95)00076-Q.

Terenzio F.G., Tilio L., Masini N.,. Murgante B., Potenza M.R., Zotta C. (2013) - *High-Detail Damage Pattern in Towns Hit by Earthquakes of the Past: An Approach to Evaluate the Reliability of the Historical Sources*. In: Bostenaru Dan M., Armas I., Goretti A. (Eds.), Earthquake Hazard Impact and Urban Planning Environmental Hazards, Springer Netherlands, pp. 105-125. doi: http://dx.doi.org/10.1007/978-94-007-7981-5_6

Tong X.H. (2012) - *Building-damage detection using pre- and post-seismic high-resolution*

satellite stereo imagery: A case study of the May 2008 Wenchuan earthquake. ISPRS Journal of Photogrammetry and Remote Sensing, 68:13-27. doi: http://dx.doi.org/10.1016/j.isprsjprs.2011.12.004.

Tronin A.A. (2006) - *Remote sensing and earthquakes: A review*. Physics and Chemistry of the Earth, 31: 138-142. doi: http://dx.doi.org/10.1016/j.pce.2006.02.024.

Turker M., Cetinkaya B. (2005) - *Automatic detection of earthquake-damaged buildings using DEMs created from pre- and post-earthquake stereo aerial photographs*. International Journal of Remote Sensing, 26: 823-832. doi: http://dx.doi.org/10.1080/01431160512331316810.

Weidner U. (1997) - *Digital surface models for building extraction*. In: Gruen A., Baltsavias E., Henricsson O. (Eds), Automatic extraction of man-made objects from aerial and space images (II). Birkhauser Verlag, Basel, pp. 193-202. doi: http://dx.doi.org/10.1007/978-3-0348-8906-3_19.

Yamazaki F. (2001) - *Applications of remote sensing and GIS for damage assessment,. Structural Safety and Reliability*. Corotis et al. (Eds), Swets&Zeitlinger, ISBN 90 5809 197 X.

Zlatanova S., Li J. (2008) - *Geospatial Information Technology for Emergency Response*. Taylor & Francis Group, London, UK, 381 p. (ISPRS book series num. 6). ISBN 13: 978-0-415-42247-5 (hbk), ISBN 13: 987-0-203-92881-3 (ebook).